Acta Pharmacologica Sinica

www.nature.com/aps

ARTICLE

Nitidine chloride induces cardiac hypertrophy in mice by targeting autophagy-related 4B cysteine peptidase

Yang Hong[1], Wan-qing Xu[1], Jing Feng[1], Han Lou[1], Heng Liu[1], Lei Wang[1], Hao Cui[1], Lin-tong Jiang[1], Ran-chen Xu[1], Heng-hui Xu[1], Min-zhen Xie[2], Yang Li[3], Philipp Kopylov[4], Qi Wang[2] and Yong Zhang[1,5,6]

Nitidine chloride (NC) is a standard active component from the traditional Chinese medicine *Zanthoxylum nitidum* (Roxb.) DC. (ZN). NC has shown a variety of pharmacological activities including anti-tumor activity. As a number of anti-tumor drugs cause cardiotoxicity, herein we investigated whether NC exerted a cardiotoxic effect and the underlying mechanism. Aqueous extract of ZN (ZNE) was intraperitoneally injected into rats, while NC was injected into beagles and mice once daily for 4 weeks. Cardiac function was assessed using echocardiography. We showed that both ZNE administered in rats and NC administered in mice induced dose-dependent cardiac hypertrophy and dysfunction, whereas administration of NC at the middle and high dose caused death in Beagles. Consistently, we observed a reduction of cardiac autophagy levels in NC-treated mice and neonatal mouse cardiomyocytes. Furthermore, we demonstrated that autophagy-related 4B cysteine peptidase (ATG4B) may be a potential target of NC, since overexpression of ATG4B reversed the cardiac hypertrophy and reduced autophagy levels observed in NC-treated mice. We conclude that NC induces cardiac hypertrophy via ATG4B-mediated downregulation of autophagy in mice. Thus, this study provides guidance for the safe clinical application of ZN and the use of NC as an anti-tumor drug.

Keywords: cardiac hypertrophy; nitidine chloride; *Zanthoxylum nitidum* (Roxb.) DC; autophagy; autophagy-related 4B cysteine peptidase; species-based differences

Acta Pharmacologica Sinica (2022) 0:1–12; https://doi.org/10.1038/s41401-022-00968-6

INTRODUCTION

Zanthoxylum nitidum (Roxb.) DC. (ZN), named Liang-Mian-Zhen in China, frequently grows in southeastern China, India, and Australia, and is a common traditional Chinese medicine with mild toxicity. It is widely used in clinical therapeutics because of its anti-inflammatory, analgesic, antibacterial, and other pharmacological effects. For example, it is one of the main ingredients of "999 Wei-Tai", a well-known Chinese patented drug for various chronic stomach diseases [1]. In addition, "Liang-Mian-Zhen" is the first toothpaste brand in China to introduce the concept of using traditional Chinese medicine to protect teeth, which is widely loved by the public [2]. ZN is rich in alkaloids, lignin, flavonoids, sterols, and other active ingredients [3]. Among them, nitidine chloride (NC), as the standard active ingredient of ZN quality control in Chinese Pharmacopeia, has attracted much attention in terms of its pharmacological and toxicological effects. Similar to ZN, NC has also been reported to have anti-inflammatory, antifungal [4], antimalarial [4], anti-human immunodeficiency viral [5], and other therapeutic effects. Interestingly and importantly, in recent years NC has been reported to present with excellent anti-tumor effects, indicating the transformation potential of NC as an anti-tumor drug [4]. Traditional Chinese medicine has made remarkable contributions to the treatment of diseases, represented by coronavirus disease-19 [6]. How to ensure the safety of traditional Chinese medicine use is crucial. With the increasing awareness of precision and personalized medicine, the cardiotoxicity of anti-tumor drugs has become a key issue in drug safety as well. So far, the nephrotoxicity and hepatotoxicity of NC have been studied [7, 8], but the cardiotoxicity of ZN and NC has not been reported.

Drug cardiotoxicity refers to the complex pathophysiological damage caused by drugs to the cardiovascular system, including cardiac hypertrophy, myocarditis, arrhythmia, myocardial ischemia, myocardial infarction, and a series of cardiac organic and functional changes. Cardiotoxicity, as one of the side effects of anti-tumor drugs, has attracted wide attention in recent years [9]. Cardiac hypertrophy, the most common manifestation of drug cardiotoxicity, is a compensatory and adaptive response of the heart to pathogenic stimuli, mainly characterized by the enlargement of myocardial cells. Without timely intervention, a well-intentioned compensation will progress to a decompensated stage, resulting in heart failure or sudden death [10]. Based on this, we systematically observed, recorded, and analyzed the cardiotoxicity and mechanism of action of ZN and its main active ingredient NC.

[1]Department of Pharmacology (the State-Province Key Laboratories of Biomedicine Pharmaceutics of China, Key Laboratory of Cardiovascular Research, Ministry of Education), College of Pharmacy, Harbin Medical University, Harbin 150081, China; [2]Department of Medicinal Chemistry and Natural Medicinal Chemistry, College of Pharmacy, Harbin Medical University, Harbin 150081, China; [3]Department of Pharmaceutical Analysis, College of Pharmacy, Harbin Medical University, Harbin 150081, China; [4]Department of Preventive and Emergency Cardiology, Sechenov First Moscow State Medical University, Moscow 101-135, Russian Federation; [5]Research Unit of Noninfectious Chronic Diseases in Frigid Zone, Chinese Academy of Medical Sciences, Harbin 150081, China and [6]Institute of Metabolic Disease, Heilongjiang Academy of Medical Science, Harbin 150086, China
Correspondence: Qi Wang (wangqiby1987@hotmail.com) or Yong Zhang (hmuzhangyong@hotmail.com)
These authors contributed equally: Yang Hong, Wan-qing Xu

Received: 15 March 2022 Accepted: 25 July 2022
Published online: 19 August 2022

© The Author(s), under exclusive licence to Shanghai Institute of Materia Medica, Chinese Academy of Sciences and Chinese Pharmacological Society 2022

Autophagy is a lysosome-dependent cellular degradation process that removes damaged or senescent intracellular components to maintain homeostasis and cellular health [11]. Autophagy is mainly mediated by microtubule-associated protein 1-light chain 3 (LC3) II, which is crucial for autophagy [12, 13]. Autophagy-related 4B cysteine peptidase (ATG4B), an enzyme encoded by the autophagy-related gene, has the highest cleavage efficiency for the conversion of pro-LC3 to LC3 I [14] and also plays a role in the conversion of LC3 II dephosphatidylethanolamine to LC3 I [15]. The maintenance of normal ATG4B levels is necessary for cellular homeostasis. Many studies have shown that autophagy is involved in the pathological mechanism of cardiac hypertrophy [16, 17]. Inhibition of ATG4B is an important factor that inhibits cardiac autophagy and causes cardiac hypertrophy [18]. In this study, we found for the first time that the level of cardiac autophagy in mice was affected by NC.

This study is the first to investigate the cardiotoxic effects of ZN and its active ingredient NC, thus providing guidance for further secure applications of traditional Chinese medicine and laying a foundation for the transformation of the active ingredients.

MATERIALS AND METHODS

Materials and reagents

NC was provided by Chengdu Pufei De Biotech Co., Ltd. (Chengdu, China). NC was dissolved in normal saline for intraperitoneal injection in animals and dissolved in dimethyl sulfoxide (DMSO) (Sigma-Aldrich, Saint Louis, MO, USA). The DMSO content did not exceed 0.1% in the final medium. Adeno-associated virus 9 (AAV9)-ATG4B (AAV9-ATG4B) and AAV9-negative control were provided by Shanghai Genechem Co., Ltd (Shanghai, China).

Animal species, groups, and ethical statements

Healthy adult male Sprague–Dawley (SD) rats (8 weeks, 200–250 g) and C57BL/6 mice (8 weeks, 20–25 g) were purchased from the Experimental Animal Center of the 2nd Affiliated Hospital of Harbin Medical University (Harbin, China). Healthy adult beagles (12–14 months, 9–12 kg) were purchased from the Shenyang Kangping Laboratory Animal Research Institute (Shenyang, China). Animals were kept in a clean, hygienic, and standardized environment. The temperature in the animal room was 23 ± 1 °C with 55% ± 5% humidity and 12 h of light and darkness. Randomization was used in all animal experiments. To test the cardiotoxicity of ZN, aqueous extract of *Zanthoxylum nitidum* (Roxb.) DC. (ZNE) was prepared, and rats were divided into four groups randomly: control, ZNE (171.38 mg/kg), ZNE (342.78 mg/kg), and ZNE (685.57 mg/kg) [19]. To test the cardiotoxicity of NC, both beagles and mice were randomly divided into four groups: beagles were divided into control and NC (0.375, 0.75, and 1.5 mg/kg) groups while mice were divided into control and NC (2.5, 5, and 10 mg/kg) groups [20]. To verify that ATG4B is a potential target of NC, mice were randomly divided into four groups: control, NC (10 mg/kg), +AAV9-ATG4B, and +AAV9-negative control. Experimental animals were injected intraperitoneally with different doses of ZNE (for rats) or NC (for beagles and mice) once a day for 4 weeks, while the control animals were administered normal saline. The weight of the animals was recorded weekly during the administration. Mice in the +AAV9-ATG4B and +AAV9-negative control groups were injected with AAV9 (1×10^{11}) via the tail vein 4 weeks earlier. All animal experiments were approved by the Ethics Committees of Harbin Medical University and conformed to the National Institutes of Health guide for the care and use of Laboratory animals (NIH Publications No. 85-23, revised 2011).

Echocardiographic assessment of cardiac function

The animals were monitored by ultrasound machines for cardiac function after a confirmation of anesthesia based on a previous study [21]. The following cardiac function-related indicators were measured: ejection fraction (EF), fractional shortening (FS), left ventricular posterior wall (LVPW) thickness, interventricular septum (IVS) thickness, left ventricular internal dimension (LVID), and left ventricular volume (LV Vol). The following ultrasound machines were used: VINNO 6 (VINNO, Suzhou, China) for rats, Esaote MyLab^{TM} (Esaote, Genoa, Italy) for beagles, and Vevo® 1100 (FUJIFILM VisualSonics, Tokyo, Japan) for mice.

Blood sample and tissue processing

After the animals were thoroughly anesthetized, blood was collected from the forelimb arteries of beagles and the abdominal aortas of rats and mice and placed in blood vessels containing ethylenediaminetetraacetic acid-K^+ (BD, Shanghai, China). After the blood was centrifuged, the plasma was subjected to liquid nitrogen rapid cooling and stored at −80 °C in a refrigerator. The whole heart was immediately removed, washed with precooled phosphate-buffered saline (PBS), drained using a filter paper, and weighed. Next, the heart was quickly cut into three parts on ice, the apex of which was placed in 2.5% glutaraldehyde (Macklin, Shanghai, China) to prepare for transmission electron microscopy, while the middle heart cavity was fixed in 4% paraformaldehyde (Biosharp, Hefei, China) to prepare for paraffin slices, followed by freezing in liquid nitrogen and then transferred to a −80 °C refrigerator for Western blot and quantitative real-time PCR analyses.

Histopathological and morphometric observation

For hematoxylin-eosin (H&E) staining, heart tissues were fixed with 4% paraformaldehyde, dehydrated, embedded in paraffin, and then sliced to a 5-μm thickness. Paraffin slices were dewaxed with xylene, hydrated with alcohol from low to high concentrations, and then stained with H&E (Beyotime, Shanghai, China). Finally, slices were dehydrated with alcohol from high to low concentrations, made transparent with xylene, covered with a coverslip, and sealed with resin as performed previously [22]. Masson staining was performed according to the kit instructions (Solarbio, Beijing, China). H&E-stained slices were imaged using a panoramic scanning microscope (Leica, Wetzlar, Germany). For transmission electron microscopy examination, heart tissue fixation and sectioning were carried out, and a JEOL 1200 electron microscope (JEOL, Tokyo, Japan) examination was performed according to previous experimental methods [22].

Immunohistochemistry assessment

Prepared heart paraffin slices were heated at 65 °C for 20 min and then exposed to xylene. Dewaxed slices were rehydrated with different concentrations of alcohol (100%, 95%, 80%, and 70%), washed with deionized water, soaked in 10 mM citric acid buffer, and heated at high temperature for 10 min without boiling. Cooled slices were washed with PBS and sealed with 3% H_2O_2 (Aladdin, Shanghai, China). After washing, slices were blocked with goat serum (Beyotime, Shanghai, China) for 1 h. Next, slices were incubated in ATG4B primary antibody ATG4B (1:100, Sigma-Aldrich, Saint Louis, MO, USA, Cat#A2981) overnight at 4 °C. On the second day, slices were incubated with horseradish peroxidase-labeled secondary antibody at room temperature for 1 h. Next, diaminobenzidine color rendering (Zhongshanjinqiao, Beijing, China) was performed. At the end of treatment with ethanol and xylene, slices were covered with coverslips and sealed with resin. The ATG4B-stained slices were imaged using a panoramic scanning microscope (Leica, Wetzlar, Germany).

Culture of neonatal mouse cardiomyocytes (NMCMs)

NMCMs were derived from newborn C57BL/6 mice with a life span of 1–3 days, as described in detail previously [23]. Animals were purchased from the Experimental Animal Center of the 2nd Affiliated Hospital of Harbin Medical University (Harbin, China).

Mixed cells obtained by digestion were cultured in high-glucose Dulbecco's modified Eagle's medium (DMEM) (HyClone, Logan, UT, USA) containing 10% fetal bovine serum (Biological Industries, Kibbutz Beit Haemek, Israel) and 1% penicillin-streptomycin solution (×100) (Beyotime, Shanghai, China) and placed in an incubator with 5% CO_2 at 37 °C. After 1.5 h, the wall of the culture flask was gently blown using a Pasteur pipette to isolate the non-adherent cardiomyocytes, while cardiac fibroblasts (CFs) were already attached to the wall. NMCMs were placed in 96- or 6-well plates for subsequent experiments. After incubation for 48 h, the NMCMs were replaced with fresh high-glucose DMEM and cultured for another 24 h before subsequent administration.

Cell counting kit-8 (CCK8) assay
Cell viability was evaluated using the CCK8 assay kit (Dojindo, Kumamoto, Japan). NMCMs or CFs were seeded into 96-well plates and treated with NC at gradient concentrations (0, 1.25, 2.5, 5, 10, 20, and 40 μM) for 24 or 48 h, as previously described [24]. After the addition of the CCK8 solution to each well (10 μL CCK8 solution/100 μL medium) and incubation for 1 h at 37 °C, absorbance was measured at 450 nm using a microplate reader.

Transfection of pcDNA3.1-ATG4B
ATG4B was cloned into the pcDNA3.1 vector to construct an ATG4B-expressing plasmid by Shanghai Abus Biotech Co., Ltd (Shanghai, China). NMCMs were transfected with the pcDNA3.1-ATG4B vector using Lipofectamine 2000 (Invitrogen, Carlsbad, CA, USA) to overexpress ATG4B, and the negative control group was transfected with an empty vector as previously described [25].

Bafilomycin A1 (BafA1) treatment and autophagic flux assay
NMCMs were treated with 10 μM NC and mRFP-GFP-LC3 adenoviral particles (HanBio, Shanghai, China) for 24 h, then added 10 nM BafA1 (MCE, Shanghai, China, Cat#HY-100558) for 24 h, the autophagic flux was photographed with a confocal microscope (LSM780, Zeiss Microsystems, Jena, Germany). NMCMs treated with NC and BafA1, but not mRFP-GFP-LC3 adenoviral particles, were used for Western blot analysis.

Protein isolation and Western blot
Protein samples were extracted from the heart/cells as previously described [25]. For heart/cellular samples, proteins were lysed using the radioimmunoprecipitation assay lysis buffer (Beyotime, Shanghai, China). After concentration determination using a bicinchoninic acid kit (Beyotime, Shanghai, China), proteins (80 μg/lane) were separated by sodium dodecyl sulfate-polyacrylamide gel electrophoresis gels (12.5%) (EpiZyme, Shanghai, China), transferred to a nitrocellulose filter membrane (Millipore Corporation, Billerica, MA, USA), and blocked with 5% skimmed milk in PBS for 2 h. Samples were incubated in primary antibodies overnight at 4 °C, followed by incubation with fluorescence-labeled secondary antibody (1:10,000, Invitrogen, Carlsbad, CA, USA) for 1 h. Fluorescence was detected using the Odyssey Imaging System (LI-COR, Lincoln, NE, USA). Primary antibodies against p62 (1:1000, Cell Signaling Technology, Boston, MA, USA, Cat#5114S), LC3 I/II (1:500, Cell Signaling Technology, Cat#12741S), ATG4B (1:500, Sigma-Aldrich, Saint Louis, MO, USA, Cat#A2981), ATG3 (1:1000, Cell Signaling Technology, Boston, MA, USA, Cat#3415S), and ATG7 (1:500, Cell Signaling Technology, Boston, MA, USA, Cat#2631S) were used. Glyceraldehyde 3-phosphate dehydrogenase (1:1000, Zhongshanjinqiao, Beijing, China, TA-08) was used as an internal control.

Cytoskeleton staining
TraKine™ F-actin Staining Kit (Green Fluorescence) (Abbkine, Wuhan, China) was used to label the cytoskeleton of NMCMs in vitro. According to the instructions, after NMCMs were fixed and penetrated, the staining solution was added to stain for 30 min (under dark condition), and finally, DAPI was dyed. The cytoskeleton of NMCMs was photographed with a confocal microscope (LSM780, Zeiss Microsystems, Jena, Germany).

Quantitative real-time PCR
RNA samples from the heart tissue and NMCMs were extracted using TRIzol reagent (Invitrogen, Carlsbad, CA, USA) according to the manufacturer's instructions. After mRNA quantification and cDNA synthesis, the level of target gene mRNA was quantified using SYBR Green I, supplied by THUNDERBIRD qPCR mix (TOYOBO, Tokyo, Japan), and quantitatively analyzed using a Roche LigthCycler® 96 SW 1.1 real-time PCR system (Roche, Mannheim, Germany), followed by a relative quantitative analysis of target mRNA [26].

Cellular thermal shift assay
NMCMs were cleaned and placed in PBS for scraping. Cell precipitates were obtained by centrifugation at 300× *g* for 3 min and resuspended in PBS. The cells were evenly divided into nine portions and heated at 43, 46, 49, 52, 55, 58, 61, 64, and 67 °C for 3 min, respectively, and then stood at room temperature for 3 min before being placed in liquid nitrogen. After repeated freeze-thaw with liquid nitrogen three times, the samples were centrifuged at 2000× *g* for 20 min. The same volume of supernatant was taken out and loading buffer (Biosharp, Hefei, China) was added. After being heated at 70 °C for 10 min, Western blot analysis was conducted.

Statistical analysis
All experimental procedures and data analysis were blinded. All data presented in this study are expressed as mean ± standard error of mean (SEM). One-way analysis of variance and Tukey's multiple-comparisons test were used for the comparative analysis between four groups or more of data. GraphPad Prism version 9.0.0 was used for all statistical analyses. $P < 0.5$ was defined as statistically significant.

RESULTS

ZN induced cardiac hypertrophy in rats
To determine whether ZN has an effect on healthy heart function, SD rats were intraperitoneally injected with different doses of ZNE. According to the prescribed dosage of ZN in Chinese pharmacopeia, the lowest and highest doses recommended clinically for adults were used as low- and middle-doses for rats, and twice the highest clinical dose was used as a high-dose for rats [19]. After 4 weeks of administration, no significant changes in the body weight of rats were observed (Fig. 1a); however, increased heart weight/body weight (HW/BW) and heart weight/tibial length (HW/TL) were observed (Fig. 1b, c). At the same time, there were some symptoms of cardiac hypertrophy (Fig. 1d), especially in the high-dose group, including upregulated EF and FS (Fig. 1e, f), thickened LVPW and IVS (Fig. 1g–j), shortened LVID during systole rather than diastole (Supplementary Fig. S1a, b), and reduced LV Vol (Supplementary Fig. S1c, d). It is worth noting that elevated LVPW thickness levels (Fig. 1g, h) both in systole and diastole were remarkable in rats administered with middle-dose ZNE, which was equivalent to the clinically recommended maximum dose of ZN. At the same time, pathological staining of hearts showed that the area of cardiomyocytes was increased in rats induced by middle- and high-dose ZNE (Fig. 1k). These results suggest that the cardiotoxicity of ZN cannot be ignored. Thus, to ensure the safety of its clinical use, it is necessary to further clarify its specific toxic components and mechanisms of action.

NC was abundant and an important component of ZN
ZN (Fig. 2a) is a traditional Chinese medicine with complex ingredients. According to the Chinese Pharmacopeia, an NC

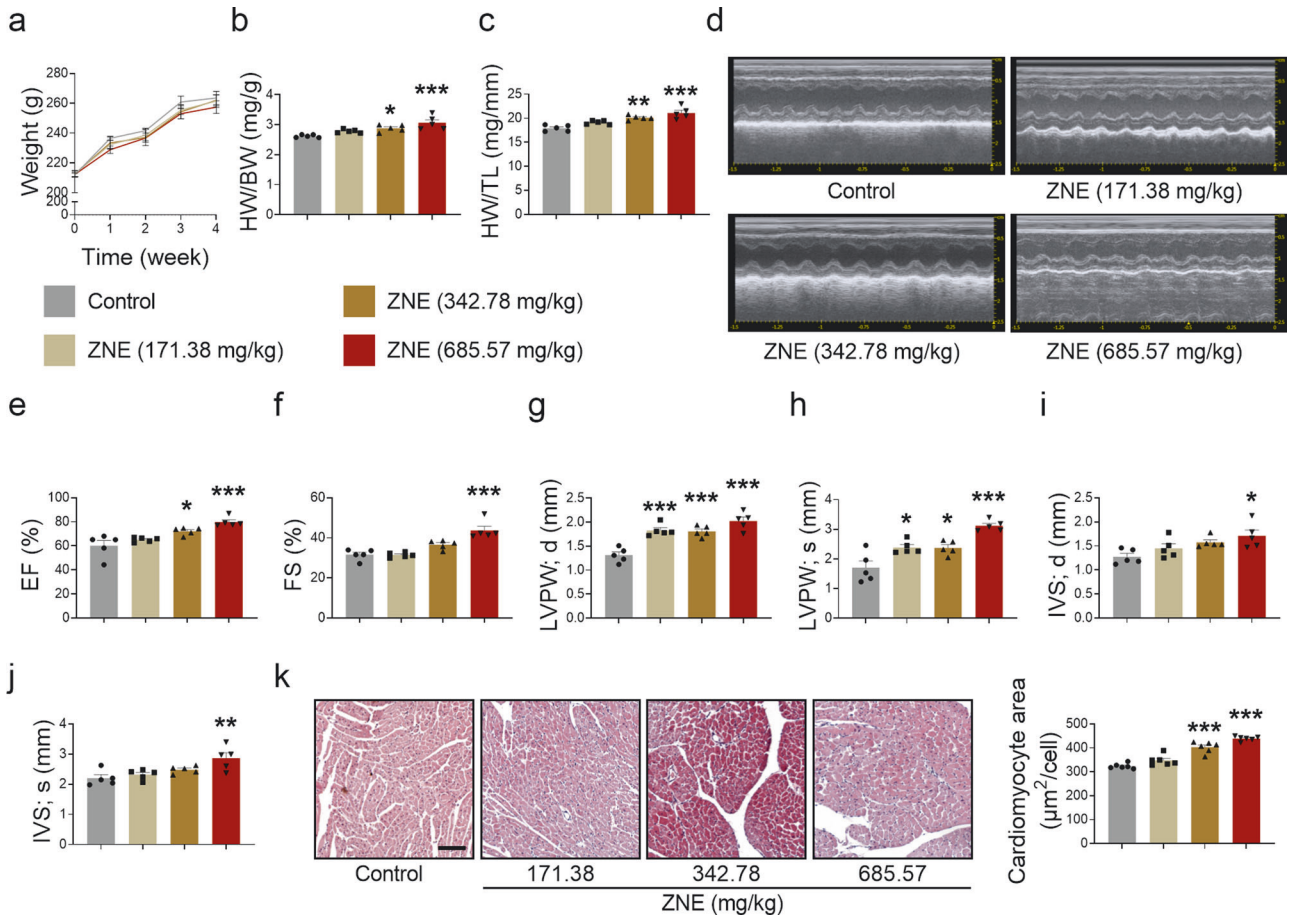

Fig. 1 ZNE induces myocardial hypertrophy in rats. Rats were intraperitoneally injected with various doses of ZNE once a day for 4 weeks. **a** Body weight changes of rats were recorded. **b**, **c** The changes in HW/BW and HW/TL were measured and counted. **d** Systolic and diastolic functions of the heart in rats were observed by echocardiography. **e**, **f** EF and FS of heart in rats were calculated. **g**, **i** LVPW thickness and IVS thickness of heart in rats were measured during diastole. **h**, **j** LVPW thickness and IVS thickness were measured during systole. **k** H&E staining (×100) of cross-sections of ventricles of rats was observed under a microscope, and the average area of a single cardiomyocyte was analyzed statistically. The red area represented cytoplasm of cardiomyocytes while the blue area represented nuclei of cardiomyocytes. Scale bar: 100 μm. $n = 5$ rats. Data are expressed as mean ± SEM, $^{*}P < 0.05$, $^{**}P < 0.01$, $^{***}P < 0.001$ vs Control.

content of (Fig. 2b) over 0.13% is defined as the quality control standard for ZN [19]. In this study, a liquid chromatography analysis of ZNE showed that the NC content was abundant (Fig. 2c). At the same time, NC was also detected in ZN by surface-enhanced Raman spectroscopy (Fig. 2d–g). After comprehensive consideration and analysis of Chinese Pharmacopeia standards and our results, NC was selected for the following experiments.

NC induced death in beagles and cardiac hypertrophy in mice

To determine the impact of NC on cardiac function, beagles, which have similar organs and blood circulation to humans, were intraperitoneally injected with different doses of NC. Death was observed in beagles in the middle- and high-dose groups from the second week of administration and within 4 weeks of administration (Fig. 3a). No significant weight changes (Fig. 3b) or cardiac abnormalities (Fig. 3c and Supplementary Fig. S2a–h) were observed in the beagles as a result of the drug, possibly due to their death.

To investigate whether NC caused cardiotoxicity rigorously, mice were exposed to different doses of NC. We found that, especially in the high-dose group, the weight of mice decreased with the prolongation of administration time (Fig. 3d), HW/BW increased (Supplementary Fig. S3a), and heart function was impaired after 4 weeks of administration (Fig. 3e), as shown by increased EF and FS (Fig. 3f, g), thickened LVPW (Fig. 3h, i), shortened LVID (Supplementary Fig. S3d, e), and decreased LV Vol (Supplementary Fig. S3f, g). However, no significant changes in IVS thickness (Supplementary Fig. S3b, c), systolic and diastolic blood pressure (Supplementary Fig. S3h, i) were observed. A histopathological analysis showed that the size of myocardial cells increased in the high-dose group (Fig. 3j). Meanwhile, we found that creatine kinase-MB (CK-MB) and aspartate aminotransferase (AST) levels in the plasma of mice were elevated in the high-dose group (Supplementary Fig. S3j, k), and the expression levels of cardiac hypertrophy related genes *β-MHC*, *ANP*, and *BNP* were increased (Supplementary Fig. S3l–n). However, myocardial fibrosis characterized by collagen deposition induced by NC was not observed (Supplementary Fig. S3o). These results suggest that high-dose NC causes myocardial hypertrophy in mice; nevertheless, the exact molecular mechanism remains unclear.

NC downregulated cardiac autophagy levels in vivo and in vitro

A proteomic analysis of surviving beagle hearts showed that, compared with the control group, mitochondrial components and peptidase activity were affected by NC in the middle- (Supplementary Fig. S4a, b) and high-dose groups (Supplementary Fig. S4c, d). Meanwhile, reduced autolysosome numbers were observed in the hearts of middle- and high-dose group mice (Fig. 4a) under transmission electron microscopy. Based on

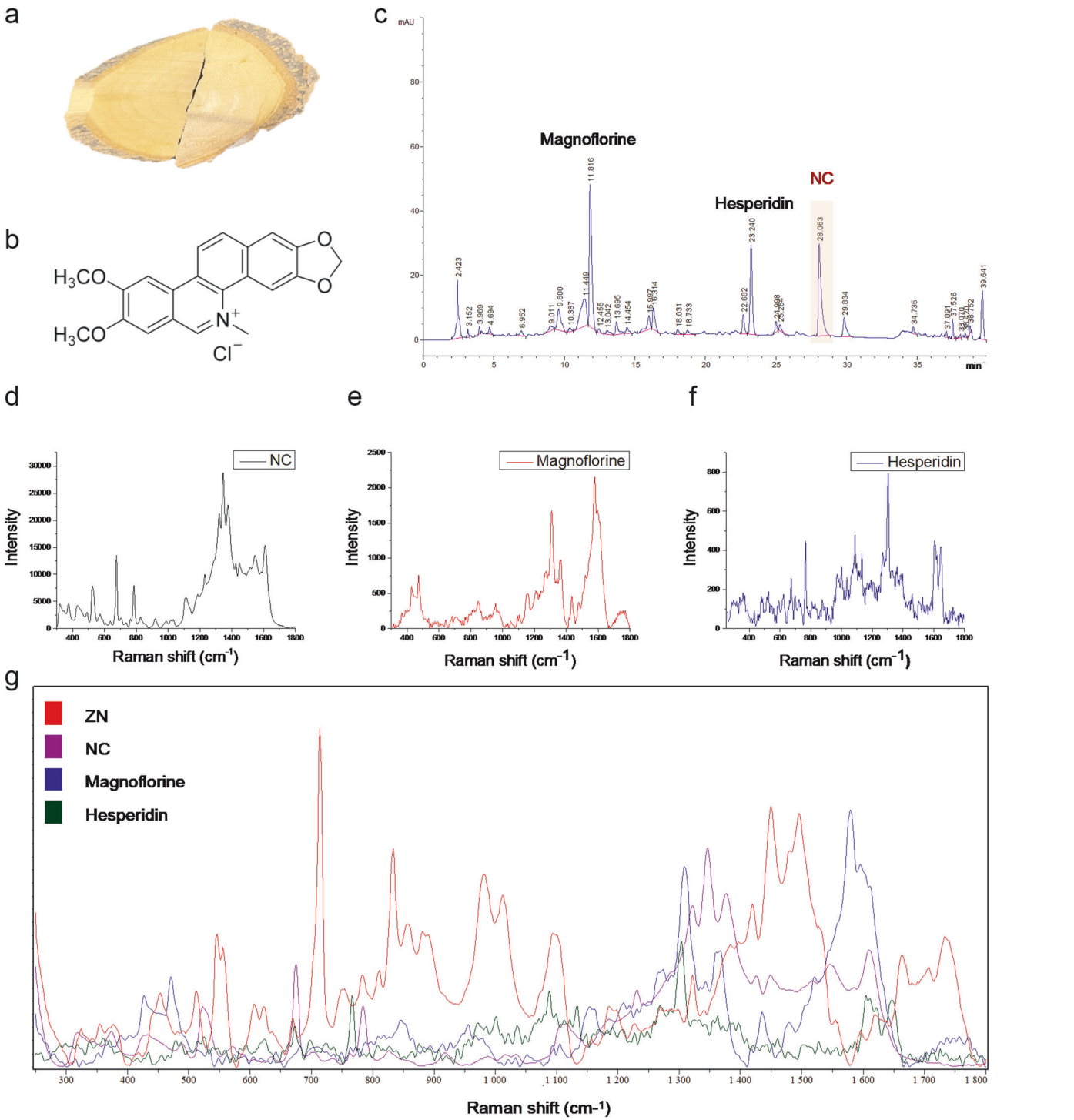

Fig. 2 Determination of NC in ZN by liquid chromatography and surface-enhanced Raman spectroscopy. a A photograph of medicinal herbs of ZN. **b** Chemical formula of NC. **c** The main active components of ZNE, including NC, magnoflorine, and hesperidin, were detected by liquid chromatography. **d**–**g** Raman shift of ZN, NC, magnoflorine, and hesperidin mixed with silver nanoparticles was obtained from the reduction of sodium borohydride and determined by surface-enhanced Raman spectroscopy.

previous study, one of the causes of myocardial cell injury is the imbalance in intracellular autophagy, a process that is closely related to mitochondria and lysosomes [27]. Thus, we further investigated whether NC affects the level of cardiac autophagy in mice. By detecting the expression levels of proteins associated with autophagy, we found that LC3 I and LC3 II protein levels significantly decreased, LC3 II/LC3 I had no significant change (Fig. 4b), while p62 levels increased (Fig. 4c) in the middle-dose and high-dose groups. At the same time, we also detected an autophagy balance in the heart of rats and found that intraperitoneal injection of middle- and high-dose ZNE also induced a decrease in the expression of LC3 I and LC3 II, non-significant changes in LC3 II/LC3 I (Supplementary Fig. S5a), and an increase in the expression of p62 (Supplementary Fig. S5b), suggesting that ZN also downregulates the level of autophagy in the heart of rats.

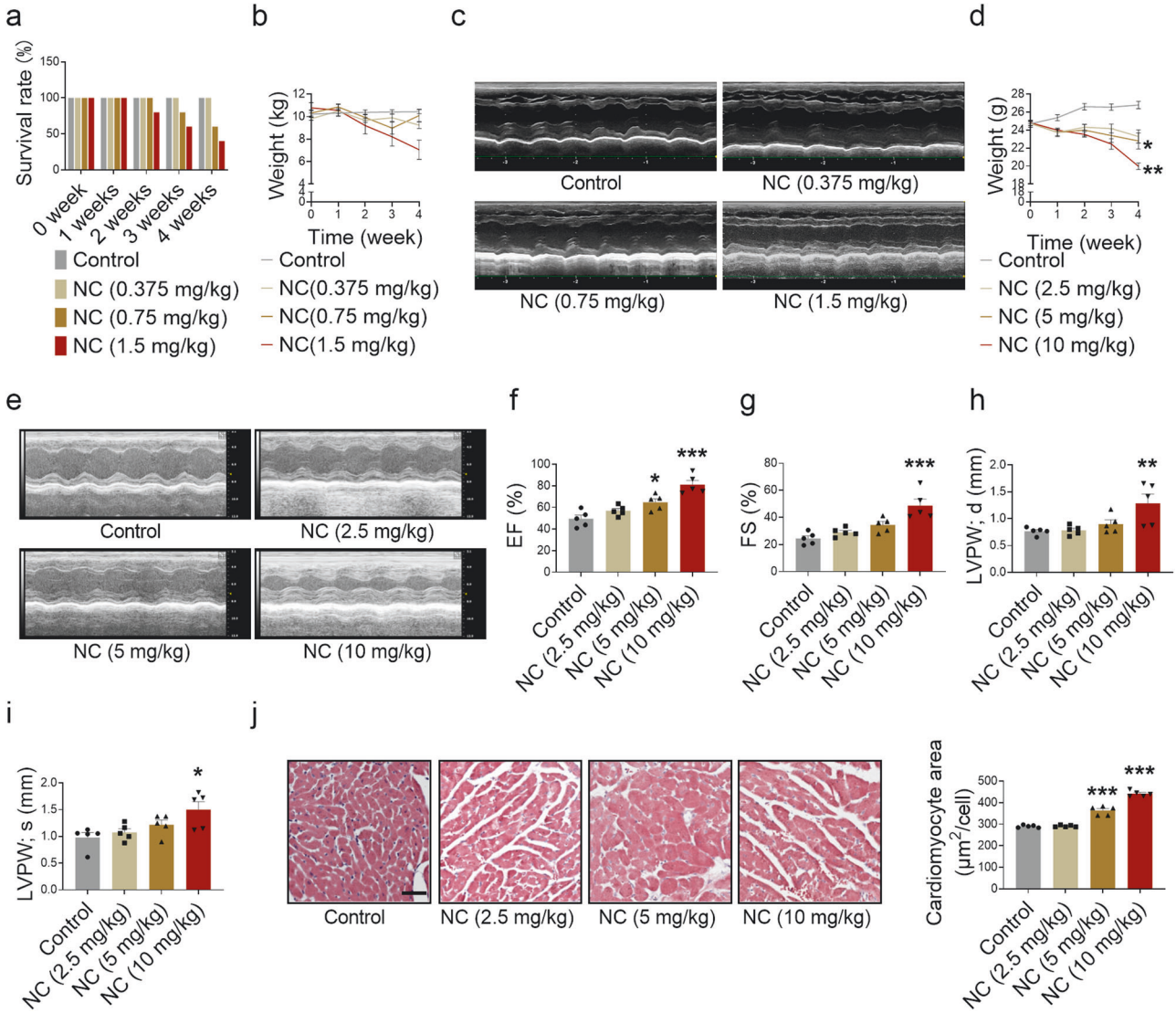

Fig. 3 Cardiotoxicity of NC in beagles and mice. Beagles were intraperitoneally injected with different doses of NC once a day for 4 weeks and anesthetized for echocardiography. **a** Beagle death rate during the 4 weeks of NC administration. **b** Body weight changes of beagles were recorded. **c** Representative images of the left heart ventricle chamber M-model were collected by echocardiography in beagles. $n = 5$ beagles in each group at week 0; $n = 5$ beagles in Control and NC (0.375 mg/kg) groups, $n = 3$ beagles in NC (0.75 mg/kg) group, and $n = 2$ beagles in NC (0.375 mg/kg) group in the fourth week. Mice were intraperitoneally injected with different doses of NC once a day for 4 weeks as well. **d** Body weight changes of mice were recorded. **e** Diastolic and systolic ultrasonic cardiogram of heart in mice. **f**–**i** The quantitative analysis of heart function changes in EF, FS, diastolic LVPW thickness, and systolic LVPW thickness in mice. **j** The sections of myocardial tissue in mice were stained with H&E (×200) after 4 weeks of NC administration, and the average area of a single cardiomyocyte was statistically analyzed. The red area represents the cytoplasm of cardiomyocytes while the blue area represents the nuclei of cardiomyocytes. Scale bar: 50 μm. $n = 5$ mice. Data are expressed as mean ± SEM, $^{*}P < 0.05$, $^{**}P < 0.01$, $^{***}P < 0.001$ vs Control.

Next, we verified the toxicity of NC to NMCMs and CFs in vitro. Our results showed that, when treated with different concentrations of NC for 24 h, the cell viability of NMCMs was significantly decreased in 40 μM NC treatment (Fig. 5a). Meanwhile, the cell viability of CFs increased after 1.25, 2.5, 5, and 10 μM NC treatment (Supplementary Fig. S6a). However, after 48 h of NC treatment, the cell viability of NMCMs dropped significantly in 1.25, 2.5, 5, 10, 20, and 40 μM NC treatment groups (Fig. 5a). And the cell viability of CFs increased in 1.25, 2.5, and 5 μM NC treatment groups, decreased in 20 and 40 μM NC treatment groups (Supplementary Fig. S6b). Based on no significant myocardial fibrosis phenotype induced by NC observed in mice (Supplementary Fig. S3o), we selected NMCMs treated with suitable NC concentrations (2.5, 5, and 10 μM) for the next experiments to verify the effect of NC on autophagy levels in NMCMs. After NC treatment for 48 h, we found an enlarged area of cardiomyocytes (Fig. 5b), decreased LC3 I and LC3 II protein expression (Fig. 5c), and increased p62 protein expression (Fig. 5d) in vitro, similarly, significant changes in LC3 II/LC3 I were not detected (Fig. 5d). In order to further clarify the regulatory role of NC on autophagy, NMCMs were treated with autophagy blocker BafA1. Compared with BafA1 group, NC (10 μM) treatment led to a decrease in LC3 I level (Supplementary Fig. S6c), no significant change in LC3 II level (Supplementary Fig. S6c) and p62 level (Supplementary Fig. S6d). Autophagic flux assay showed that NC treatment promoted the decrease of autophagy level in both untreated and BafA1-induced NMCMs (Fig. 5e). The results of in vitro experiments suggest that NC leads to cardiotoxicity by downregulating autophagy levels in cardiomyocytes; however, the exact molecular target is unclear.

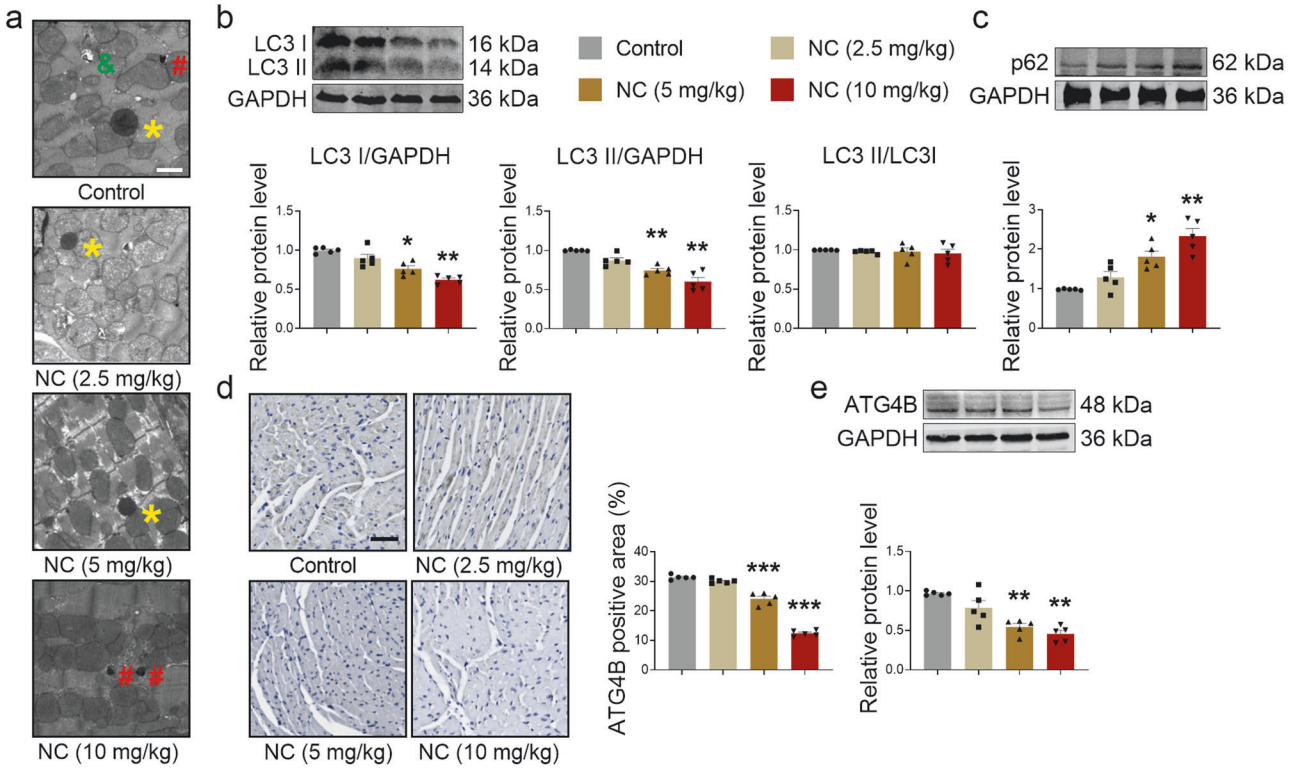

Fig. 4 NC downregulates the level of cardiac autophagy in vivo. Mice were intraperitoneally injected with different doses of NC once a day for 4 weeks. **a** The number of autophagic lysosomes in the hearts of mice was observed by transmission electron microscopy (×2500) after 4 weeks of administration, * for autolysosome, # for lysosome, & for autophagosome. Scale bar: 2 μm. $n = 3$ mice. **b**, **c** The expression levels of autophagy-related proteins LC3 I, LC3 II, LC3 II/LC3 I, and p62 of hearts in mice were determined by Western blot analysis after 4 weeks of administration. **d** Immunohistochemical staining (×200) of ATG4B of the cross-section of hearts in mice was observed under a microscope, and ATG4B positive area was statistically analyzed. Scale bar: 50 μm. **e** Relative expression level of ATG4B protein in vivo was measured by Western blot analysis. $n = 5$ mice. Data are expressed as mean ± SEM, $^{*}P < 0.05$, $^{**}P < 0.01$, $^{***}P < 0.001$ vs Control.

As a potential target of NC, overexpression of ATG4B alleviated NC-induced cardiac hypertrophy

Based on the experimental results showing that both LC3 I and LC3 II protein levels decreased after NC treatment and the mechanism by which LC3 II was converted from LC3 I, we further explored how NC affected LC3 I protein expression. Studies have shown that LC3 I is converted from pro-LC3 with the participation of ATG4B [28], and the proteomic analysis of the heart of beagles also suggested that NC might regulate peptidase activity. Thus, we hypothesized that NC may regulate autophagy by targeting ATG4B. To test this hypothesis, ATG4B protein expression levels were monitored both in vivo and in vitro. Immunohistochemical staining showed that ATG4B expression gradually decreased with an increasing NC dose (Fig. 4d). ATG4B expression, as determined by Western blot, also verified that NC decreased ATG4B protein expression in vivo (Fig. 4e). Similarly, decreased expression levels of ATG4B protein induced by NC were also confirmed in vitro (Fig. 5f). In addition, the expression levels of ATG3 and ATG7, two other autophagy-related proteins involved in the transformation between LC3 I and LC3 II [29], were not affected by NC (Supplementary Fig. S6e, f). Therefore, ATG4B may be a potential target for NC to regulate cardiac autophagy.

To further confirm that NC regulates LC3 I by targeting ATG4B, mice treated with NC were administered AAV9-ATG4B via the tail vein to overexpress ATG4B for 4 weeks in advance. We found that overexpression of ATG4B alleviated the changes in the weight and HW/BW induced by NC administration for 4 weeks (Fig. 6a and Supplementary Fig. S7a). Most importantly, overexpression of ATG4B improved the cardiac function of mice treated with NC (Fig. 6b), including recovered EF, FS, and LVPW thickness (Fig. 6c–f). Again, no significant changes in IVS thickness were observed (Supplementary Fig. S7b, c); however, significant recovery in LVID and LV Vol was observed (Supplementary Fig. S7d–g). In addition, improvement in cardiac hypertrophy induced by NC was observed by H&E staining (Fig. 6g). Improved markers of heart injury, such as CK-MB and AST levels (Supplementary Fig. S7h, i), and alleviated expression levels of genes associated with cardiac hypertrophy, including *β-MHC, ANP*, and *BNP* were observed (Supplementary Fig. S7i–l). Consistent with our previous results, the myocardial fibrosis phenotype reflected by the Masson staining was not observed (Supplementary Fig. S7m). These results indicate that overexpression of ATG4B improves NC-induced cardiac hypertrophy.

Overexpression of ATG4B restored autophagy levels affected by NC both in vivo and in vitro

To verify the relationship between NC, ATG4B, and autophagy, we examined the changes in autophagy levels in mice. Firstly, the expression level of ATG4B protein was detected by immunohistochemistry and Western blot to confirm the successful overexpression of ATG4B (Fig. 7a, b). Next, transmission electron microscopy imaging of heart sections showed that overexpression of ATG4B restored autophagosome formation, which was inhibited by NC (Fig. 7c). Western blot analysis revealed that overexpression of ATG4B significantly reversed the decline in autophagy caused by NC, which was manifested by increased LC3 I and LC3 II expression levels, unchanged LC3 II/LC3 I and decreased p62 expression levels (Fig. 7d, e).

In addition, we overexpressed ATG4B in NMCMs before NC treatment to verify the regulatory effect of NC on ATG4B (Fig. 8a). Using the CCK8 assay we found that ATG4B overexpression protected against NC-induced effects on cell viability (Fig. 8b).

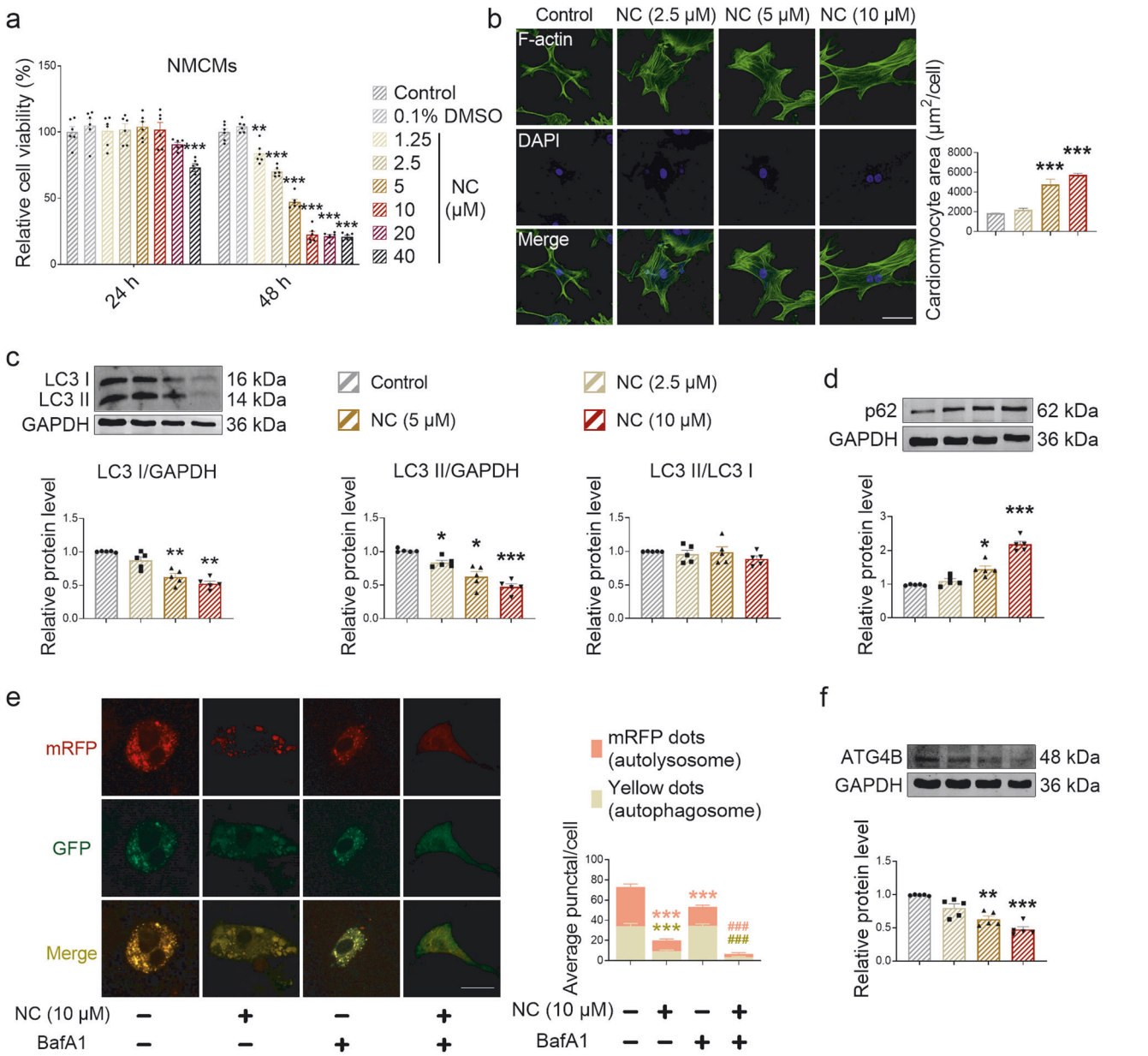

Fig. 5 NC induces cardiomyocyte hypertrophy by downregulating autophagy level in vitro. NMCMs inoculated in 96-well plates were treated with different concentrations of NC for 24 or 48 h. **a** CCK8 was used to detect cell viability of NMCMs after NC treatment for 24 or 48 h. $n = 6$ cells. NMCMs were treated with different concentrations of NC treatment for 48 h. **b** The cytoskeleton of NMCMs was stained with F-actin, and the area of a single cardiomyocyte was statistically analyzed. Scale bar: 50 μm. $n = 3$ cells. **c**, **d** The expression levels of autophagy-related proteins LC3 I, LC3 II, LC3 II/LC3 I, and p62 of NMCMs were detected by Western blot analysis after different concentrations of NC treatment for 48 h. $n = 5$ cells. **e** Autophagosomes (yellow dots) and autolysosomes (red dots) were measured and statistically analyzed. Scale bar: 20 μm. $n = 5$ cells. **f** Relative expression level of ATG4B protein was measured by Western blot analysis. $n = 5$ cells. Data are expressed as mean ± SEM, $^{*}P < 0.05$, $^{**}P < 0.01$, $^{***}P < 0.001$ vs Control. $^{\#\#\#}P < 0.001$ vs BafA1.

Importantly, overexpression of ATG4B restored NC-induced cardiomyocyte area enlargement (Fig. 8c). The Western blot analysis showed that overexpression of ATG4B inhibited the decline in LC3 I, and LC3 II levels and the increase in p62 level caused by NC (Fig. 8d, e).

As for the mechanism of NC regulating ATG4B protein expression, since ATG4B plays a physiological role by forming a complex with LC3 [30], we speculated whether NC would interfere with the formation of ATG4B-LC3 complex. SYBYL 2.0 software was used to conduct molecular docking between NC and ATG4B-LC3 complex (2Z0D) (Supplementary Fig. S8a). The results showed that NC could bind to the A/ASN261 site of ATG4B protein in the ATG4B-LC3 complex (Supplementary Fig. S8b). The calculated CScore of 4 and Polar value of 0.03 indicate optimal polar interaction between NC and ATG4B, and Crash value of −1.78 reflects the degree of intermolecular collision. Furthermore, the binding relationship between NC and ATG4B was verified by cellular thermal shift assay (Supplementary Fig. S8c). This result suggests that NC may interfere with the formation of ATG4B-LC3 complex by binding with ATG4B, resulting in the degradation of ATG4B due to its inability to perform normal physiological functions. These results demonstrate NC inhibits cardiac autophagy by downregulating ATG4B protein expression levels, resulting in cardiac hypertrophy and cardiotoxicity in mice.

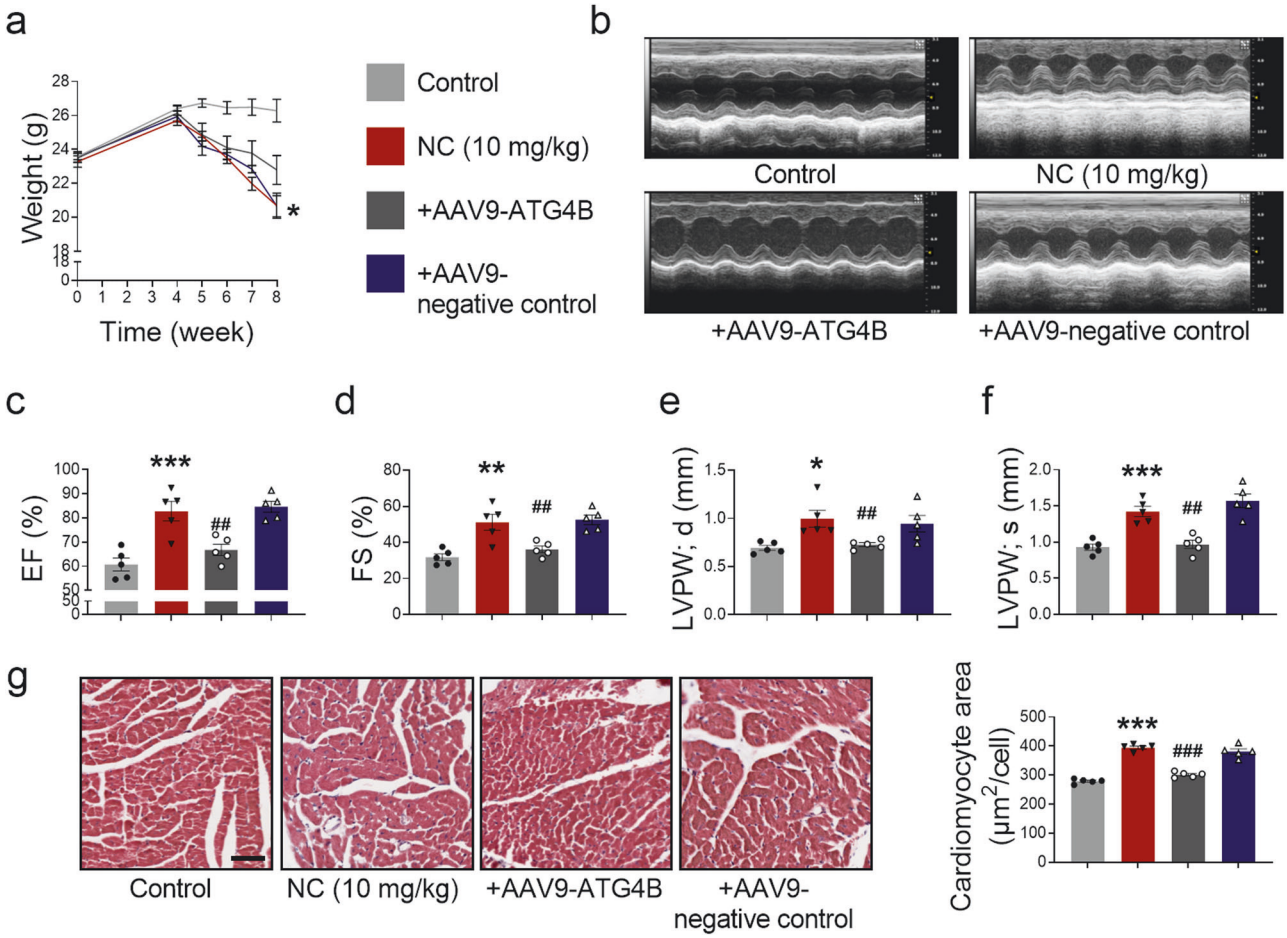

Fig. 6 Overexpression of ATG4B rescues NC-induced cardiac hypertrophy in mice. Mice in ATG4B overexpression group and negative control group were injected with AAV9-ATG4B and AAV9-negative control by tail vein, respectively. Four weeks later, mice in the experimental group, ATG4B overexpression group, and negative control group suffered from NC intraperitoneal injection once a day for 4 weeks. **a** The initial body weight and the weight changes of mice within 4 weeks of NC administration were recorded in detail. **b** Cardiac function in diastolic and systolic stages of mice with or without AAV9-ATG4B was recorded by echocardiography. **c**–**f** Quantitation analyses of heart function changes in EF, FS, diastolic LVPW thickness, and systolic LVPW thickness in mice. **g** Pathological changes in myocardial tissue were observed by H&E staining (×200) in mice, and the average area of a single cardiomyocyte was statistically analyzed. Scale bar: 50 μm. $n = 5$ mice. Data are expressed as mean ± SEM, $^{*}P < 0.05$, $^{**}P < 0.01$, $^{***}P < 0.001$ vs Control. $^{\#\#}P < 0.01$, $^{\#\#\#}P < 0.001$ vs NC (10 mg/kg).

DISCUSSION

This study presented three main novel findings: (1) ZN induced cardiac toxicity in rats, (2) NC induced cardiac toxicity in mice, and (3) ATG4B was identified as a target of NC for the regulation of autophagy, which is an underlying mechanism for the cardiac toxicity of ZN and NC. This study provides new findings related to the cardiotoxicity of ZN and NC, thus contributing to the safe clinical application of ZN and the transformation of NC as an anti-tumor drug.

Known as a mildly toxic herb, ZN has been used for thousands of years for its therapeutic properties for the treatment of toothache, neuralgia, sore throat, snake bite, and others [31]. In order to adapt to the modern development trend of traditional Chinese medicine, we hope to master the pharmacological and toxicological properties of drugs as much as possible. Therefore, we focused on exploring whether ZN presents with cardiotoxicity under existing pharmacopeia guidance. We found that, under the maximum clinical dose, ZN induced myocardial hypertrophy in rats, thus providing evidence of the risks of clinical application of ZN. However, the complex composition of ZN presents a new challenge to elucidate its cardiotoxic effects and mechanisms. Thus, to clarify the cardiotoxic mechanism of ZN, NC, as the most important active ingredient in Chinese pharmacopoeia for the quality control of ZN, was adopted for further study.

With the development of modern medicine, an increasing number of traditional Chinese medicines and their active ingredients have been found to have new pharmacodynamics [32]. Some traditional Chinese medicine monomers have attracted great attention because of their excellent anti-tumor effects and have therefore become candidates for anti-tumor drug therapy [33]. NC, a traditional Chinese medicine, has been widely reported for its excellent anti-tumor activities over the past decade, including hepatocellular carcinoma [34], ovarian cancer [35], prostate cancer [36], and others. In summary, NC has inhibitory effects on a variety of tumors. At the same time, the toxicity of anti-tumor drugs has always been a difficult problem to solve, and cardiotoxicity has been of particular concern for the last few years. For both the clinical application of ZN and the transformation potential of NC as an anti-tumor drug, the toxic effect is second only to their clinical therapeutic effects, which attract the most attention.

As a vital organ for maintaining human life, the heart is often a target of drug-induced toxicity. It is important for clinicians and clinical pharmacists to have a good understanding of the pharmacological and toxicological properties of drugs and to

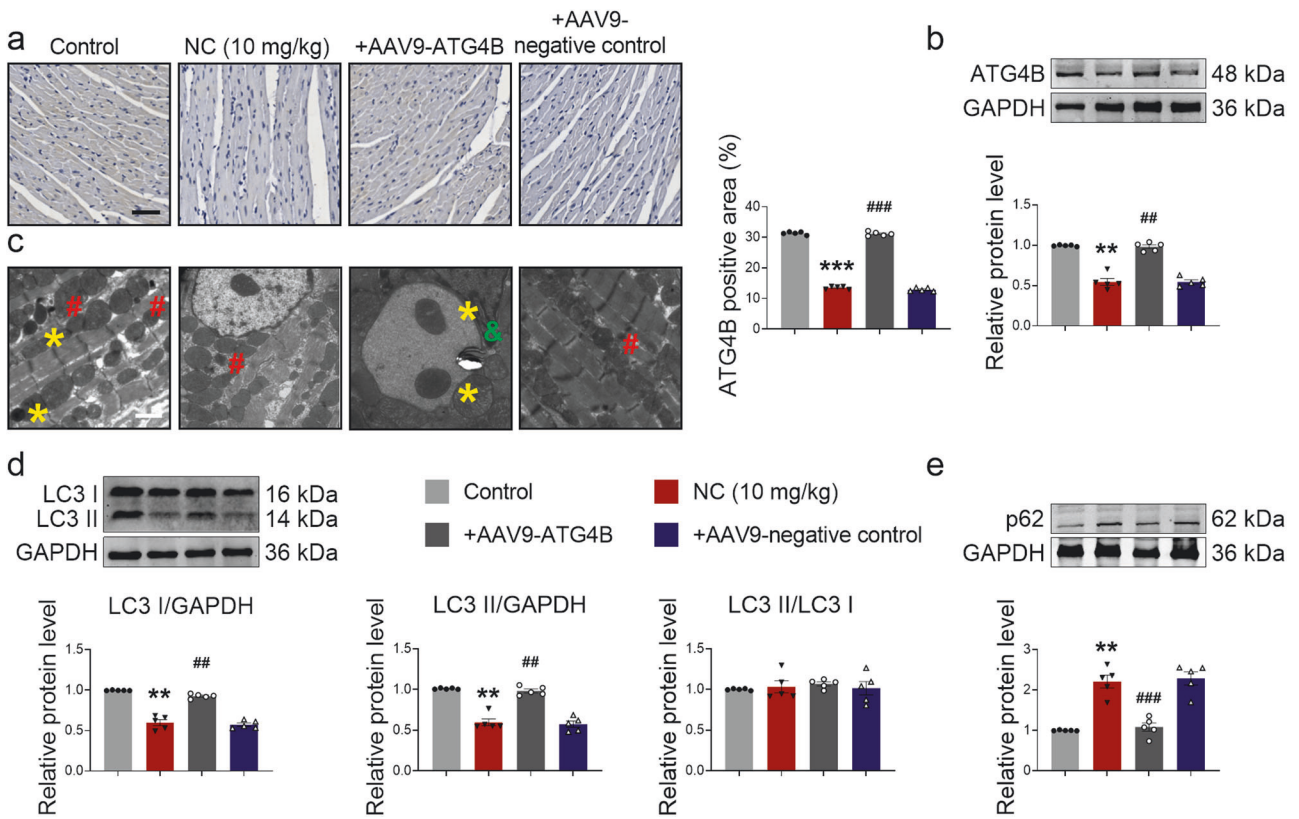

Fig. 7 Overexpression of ATG4B improves NC-induced decrease in autophagy levels in vivo. Mice in the ATG4B overexpression group and negative control group were injected with AAV9-ATG4B and AAV9-negative control via the tail vein, respectively. Four weeks later, mice in the experimental group, ATG4B overexpression group, and negative control group received NC via intraperitoneal injection once a day for 4 weeks. **a** Immunohistochemical staining (×200) of ATG4B of the cross-section of hearts in mice was observed under a microscope, and ATG4B positive area was statistically analyzed. Scale bar: 50 μm. $n = 5$ mice. **b** The expression level of ATG4B protein was detected by Western blot in the hearts of mice. $n = 5$ mice. **c** Autophagosomes in the hearts of mice were imaged under transmission electron microscopy (×2500), * for autolysosome, # for lysosome, & for autophagosome. Scale bar: 2 μm. $n = 3$ mice. **d**, **e** Western blot analysis showed changes in the expression levels of autophagy-related proteins LC3 I, LC3 II, LC3 II/LC3 I, and p62 in the hearts of mice. $n = 5$ mice. Data are expressed as mean ± SEM, $^{**}P < 0.01$, $^{***}P < 0.001$ vs Control. $^{\#\#}P < 0.01$, $^{\#\#\#}P < 0.001$ vs NC (10 mg/kg).

ensure that drugs are properly administered to patients to perform their therapeutic effects without causing new risks. Arsenic trioxide (As_2O_3) is not only an effective drug against acute promyelocytic leukemia but also a highly toxic drug, and extreme caution should be taken when considering its clinical application. Our research group previously reported that As_2O_3 can lead to myocardial fibrosis by inducing endothelial to mesenchymal transition, which suggests that clinicians should pay attention to cardiac function when administering arsenic trioxide to patients with leukemia and also provide a theoretical basis for patients to achieve good clinical outcomes while avoiding adverse reactions [37]. Due to its anti-inflammatory and analgesic effects, ZN has also played an important role in traditional Chinese medicine for thousands of years, with NC becoming a "rising star" among anti-tumor monomers. Thus, our aim was to investigate the cardiotoxic effects and mechanisms of NC.

To explore the cardiotoxicity of NC, we calculated the dose of NC in beagles and mice based on the body surface area of the different species. Using the same treatment dose, we found species-based differences in NC-induced toxicity between beagles and mice. Beagles in the high-dose group began to die 2 weeks after administration, as did those in the medium-dose group 3 weeks after administration. However, no mice died during the 4 weeks of administration. In addition, there was no significant change in cardiac function in the surviving beagles at the end of 4 weeks of administration, whereas significant cardiac hypertrophy was observed in mice in the high-dose group. This result illustrates differences in the toxic reactivity to NC between beagles and mice. We are interested in exploring the causes of this difference in detail in future studies. Previous studies on species diversity may help us generate new ideas and understand whether humans and animals have such species diversity [38]. However, NC-induced nephrotoxicity and hepatotoxicity have been reported in previous studies [7, 8]. Furthermore, we have also confirmed the cardiotoxicity of NC, which is enough to support the need for strict indications for the clinical use of NC if used as an anti-tumor agent. In summary, our research ideas have far-reaching implications for the safe use of NC in cancer patients with heart diseases.

In this study we revealed the effect of NC on cardiac autophagy homeostasis. Autophagy is an evolutionarily conserved process that facilitates cellular homeostasis by metabolizing old, damaged organelles and misfolded proteins to fuel new cellular metabolism [39]. In particular, adenosine triphosphate produced via autophagy during intracellular material degradation and recycling is essential for cardiomyocytes, which require a large amount of energy to function [40]. Autophagy maintains cardiovascular homeostasis and its absence can lead to cardiovascular diseases [41]. Although extensive studies have been conducted on the pharmacological mechanisms of NC, to date, there is no research on whether NC affects the level of autophagy. Our study is the first to show that NC affects cardiac autophagy levels. During the autophagy process, LC3 II is obtained by combining LC3 I with phosphatidylethanolamine with the

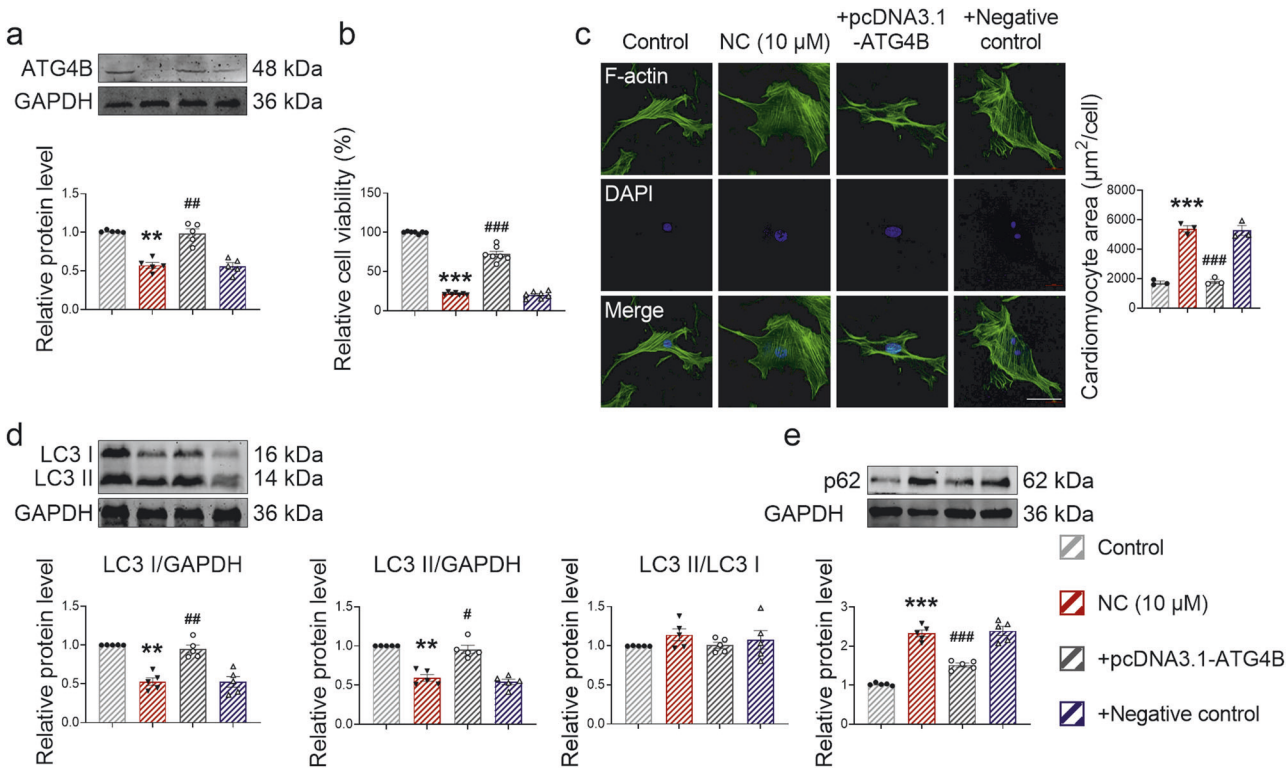

Fig. 8 NC regulates autophagy by targeting ATG4B, affecting cardiomyocyte hypertrophy. a After NMCMs were transfected with ATG4B for 48 h, the overexpression efficiency of ATG4B was verified by Western blot. $n = 5$ cells. NMCMs were transfected with ATG4B for 24 h and treated with NC for 48 h. **b** The cell viability was determined using the CCK8 kit. $n = 7$ cells. **c** The cytoskeleton of NMCMs was stained with F-actin, and the area of a single cardiomyocyte was statistically analyzed. Scale bar: 50 μm. $n = 3$ cells. **d**, **e** The expression levels of autophagy-related proteins LC3 I, LC3 II, LC3 II/LC3 I, and p62 in NMCMs were quantified by Western blot analysis. $n = 5$ cells. Data are expressed as mean ± SEM, $^{**}P < 0.01$, $^{***}P < 0.001$ vs Control. $^{\#}P < 0.05$, $^{\#\#}P < 0.01$, $^{\#\#\#}P < 0.001$ vs NC (10 μM).

participation of ATG12-ATG5, while LC3 I, an important executor of autophagy, is obtained via ATG4B-mediated cleavage of pro-LC3 [42]. Based on the results showing that NC induced changes in the protein expression levels of LC3 I, we speculated that NC might regulate autophagy in cardiomyocytes via the targeting of ATG4B, a hypothesis that was confirmed by subsequent ATG4B overexpression experiments, and the binding relationship between NC and ATG4B was verified by cellular thermal shift assay. It has been reported that LC3 II can be reconverted to LC3 I after ATG4B processing [15]. The bidirectional regulation of ATG4B on LC3 I might also offer an explanation for why there is little difference in protein expression changes between LC3 I and LC3 II, both LC3 I and LC3 II declined after NC treatment, instead of a decrease in LC3 II was more obvious. Thus, coinciding with the previously described anti-tumor effect of NC [4], the results of this study show the potential of ATG4B inhibitors for tumor treatment. Although there are no studies on the effect of NC on autophagy levels, this study lays the foundation for linking NC with the mechanism of autophagy.

In this study, we found that the highest clinically recommended dose of ZN caused cardiac hypertrophy. NC, as the standard active component of ZN, downregulates cardiac autophagy by targeting ATG4B, which in turn causes cardiac hypertrophy. Thus, this study enriches the existing literature on the cardiac toxicity of ZN and NC and provides guidance for a safe clinical application of ZN and the use of NC as a potential anti-tumor drug.

ACKNOWLEDGEMENTS

This work was supported by the National Key R&D Program of China (grant number 2017YFC1702003).

AUTHOR CONTRIBUTIONS

YZ proposed the conception for the study; QW designed the experiments; YH and QW wrote the paper; YH and WQX performed research and analyzed data; JF, Han Lou, Heng Liu, LW, HC, LTJ, RCX, HHX, MZX, YL, and PK performed research; QW and YH gave critical discussions and revisions on the paper.

ADDITIONAL INFORMATION

Supplementary information The online version contains supplementary material available at https://doi.org/10.1038/s41401-022-00968-6.

Competing interests: The authors declare no competing interests.

REFERENCES

1. Lu Q, Li CL, Wu GS. Insight into the inhibitory effects of *Zanthoxylum nitidum* against *Helicobacter pylori* urease and jack bean urease: kinetics and mechanism. J Ethnopharmacol. 2020;249:112419.
2. Liu Q, Wang T, Zhou L, Song F, Qin A, Feng HT, et al. Nitidine chloride prevents OVX-induced bone loss via suppressing NFATc1-mediated osteoclast differentiation. Sci Rep. 2016;6:36662.
3. Lin Q, Pu H, Guan H, Ma C, Zhang Y, Ding W, et al. Rapid identification and pharmacokinetic studies of multiple active alkaloids in rat plasma through UPLC-Q-TOF-MS and UPLC-MS/MS after the oral administration of *Zanthoxylum nitidum* extract. J Pharm Biomed Anal. 2020;186:113232.
4. Cui Y, Wu L, Cao R, Xu H, Xia J, Wang ZP, et al. Antitumor functions and mechanisms of nitidine chloride in human cancers. J Cancer. 2020;11:1250–6.
5. Mitrasinovic PM. Structural insights into the binding of small ligand molecules to a G-quadruplex DNA located in the HIV-1 promoter. J Biomol Struct Dyn. 2018;36:2292–302.
6. Lyu M, Fan G, Xiao G, Wang T, Xu D, Gao J, et al. Traditional Chinese medicine in COVID-19. Acta Pharm Sin B. 2021;11:3337–63.
7. Li LP, Song FF, Weng YY, Yang X, Wang K, Lei HM, et al. Role of OCT2 and MATE1 in renal disposition and toxicity of nitidine chloride. Br J Pharmacol. 2016;173:2543–54.

8. Li L, Tu M, Yang X, Sun S, Wu X, Zhou H, et al. The contribution of human OCT1, OCT3, and CYP3A4 to nitidine chloride–induced hepatocellular toxicity. Drug Metab Dispos. 2014;42:1227–34.
9. Bradley R, Braybrooke J, Gray R, Hills R, Liu Z, Peto R, et al. Trastuzumab for early-stage, HER2-positive breast cancer: a meta-analysis of 13 864 women in seven randomised trials. Lancet Oncol. 2021;22:1139–50.
10. Deng KQ, Wang A, Ji YX, Zhang XJ, Fang J, Zhang Y, et al. Suppressor of IKKε is an essential negative regulator of pathological cardiac hypertrophy. Nat Commun. 2016;7:1–21.
11. Wang Y, Que H, Rong Y. Autophagosomal components recycling on autolysosomes. Trends Cell Biol. 2022;12:S0962–8924. 00151-9
12. Li HM, Liu X, Meng ZY, Wang L, Zhao LM, Chen H, et al. Kanglexin delays heart aging by promoting mitophagy. Acta Pharmacol Sin. 2022;43:613–23.
13. Chen XL, Liu P, Zhu WL, Lou LG. DCZ5248, a novel dual inhibitor of Hsp90 and autophagy, exerts antitumor activity against colon cancer. Acta Pharmacol Sin. 2021;42:132–41.
14. Skytte Rasmussen M, Mouilleron S, Kumar Shrestha B, Wirth M, Lee R, Bowitz Larsen K, et al. ATG4B contains a C-terminal LIR motif important for binding and efficient cleavage of mammalian orthologs of yeast Atg8. Autophagy. 2017;13:834–53.
15. Huang T, Wan X, Alvarez AA, James CD, Song X, Yang Y, et al. MIR93 (microRNA-93) regulates tumorigenicity and therapy response of glioblastoma by targeting autophagy. Autophagy. 2019;15:1100–11.
16. Liu CY, Zhang YH, Li RB, Zhou LY, An T, Zhang RC, et al. LncRNA CAIF inhibits autophagy and attenuates myocardial infarction by blocking p53-mediated myocardin transcription. Nat Commun. 2018;9:1–12.
17. Liu B, Li L, Liu G, Ding W, Chang W, Xu T, et al. Baicalein attenuates cardiac hypertrophy in mice via suppressing oxidative stress and activating autophagy in cardiomyocytes. Acta Pharmacol Sin. 2021;42:701–14.
18. Zhang Y, Ding Y, Li M, Yuan J, Yu Y, Bi X, et al. MicroRNA-34c-5p provokes isoprenaline-induced cardiac hypertrophy by modulating autophagy via targeting ATG4B. Acta Pharm Sin B. 2022;12:2374–90.
19. Commission Chinese Pharmacopoeia. Pharmacopoeia of the People's Republic of China. Beijing, China: China Medical Science Press; 2020.
20. Liu LM, Xiong DD, Lin P, Yang H, Dang YW, Chen G. DNA topoisomerase 1 and 2A function as oncogenes in liver cancer and may be direct targets of nitidine chloride. Int J Oncol. 2018;53:1897–912.
21. Zhang Y, Jiao L, Sun L, Li Y, Gao Y, Xu C, et al. LncRNA ZFAS1 as a SERCA2a inhibitor to cause intracellular Ca^{2+} overload and contractile dysfunction in a mouse model of myocardial infarction. Circ Res. 2018;122:1354–68.
22. Li Z, Xu H, Liu X, Hong Y, Lou H, Liu H, et al. GDF11 inhibits cardiomyocyte pyroptosis and exerts cardioprotection in acute myocardial infarction mice by upregulation of transcription factor HOXA3. Cell Death Dis. 2020;11:1–10.
23. Zhang Y, Sun L, Xuan L, Pan Z, Hu X, Liu H, et al. Long non-coding RNA CCRR controls cardiac conduction via regulating intercellular coupling. Nat Commun. 2018;9:4176.
24. Ding F, Liu T, Yu N, Li S, Zhang X, Zheng G, et al. Nitidine chloride inhibits proliferation, induces apoptosis via the Akt pathway and exhibits a synergistic effect with doxorubicin in ovarian cancer cells. Mol Med Rep. 2016;14:2853–9.
25. Zhang Y, Liu X, Bai X, Lin Y, Li Z, Fu J, et al. Melatonin prevents endothelial cell pyroptosis via regulation of long noncoding RNA MEG3/miR-223/NLRP3 axis. J Pineal Res. 2018;64:e12449.
26. Bai X, Yang C, Jiao L, Diao H, Meng Z, Wang L, et al. LncRNA MIAT impairs cardiac contractile function by acting on mitochondrial translocator protein TSPO in a mouse model of myocardial infarction. Signal Transduct Target Ther. 2021;6:172.
27. Xu M, Wan CX, Huang SH, Wang HB, Fan D, Wu HM, et al. Oridonin protects against cardiac hypertrophy by promoting P21-related autophagy. Cell Death Dis. 2019;10:1–16.
28. Agrotis A, Pengo N, Burden JJ, Ketteler R. Redundancy of human ATG4 protease isoforms in autophagy and LC3/GABARAP processing revealed in cells. Autophagy. 2019;15:976–97.
29. Frudd K, Burgoyne T, Burgoyne JR. Oxidation of Atg3 and Atg7 mediates inhibition of autophagy. Nat Commun. 2018;9:95.
30. Satoo K, Noda NN, Kumeta H, Fujioka Y, Mizushima N, Ohsumi Y, et al. The structure of Atg4B–LC3 complex reveals the mechanism of LC3 processing and delipidation during autophagy. EMBO J. 2009;28:1341–50.
31. Hu J, Shi X, Mao X, Chen J, Li H. Cytotoxic mannopyranosides of indole alkaloids from *Zanthoxylum nitidum*. Chem Biodivers. 2014;11:970–4.
32. Xiong H, Zhang AH, Guo YJ, Zhou XH, Sun H, Yang L, et al. A clinical and animal experiment integrated platform for small-molecule screening reveals potential targets of bioactive compounds from a herbal prescription based on the therapeutic efficacy of Yinchenhao Tang for jaundice syndrome. Engineering. 2021;7:1293–305.
33. Xiang YC, Shen J, Si Y, Liu XW, Zhang L, Wen J, et al. Paris saponin VII, a direct activator of AMPK, induces autophagy and exhibits therapeutic potential in non-small-cell lung cancer. Chin J Nat Med. 2021;19:195–204.
34. Xiong D, Feng Z, Lai Z, Qin Y, Liu L, Fu H, et al. High throughput circRNA sequencing analysis reveals novel insights into the mechanism of nitidine chloride against hepatocellular carcinoma. Cell Death Dis. 2019;10:1–16.
35. Chen SP, Yang L, Feng J. Nitidine chloride inhibits proliferation and induces apoptosis in ovarian cancer cells by activating the Fas signalling pathway. J Pharm Pharmacol. 2018;70:778–86.
36. Shi Y, Cao T, Sun Y, Xia J, Wang P, Ma J. Nitidine chloride inhibits cell proliferation and invasion via downregulation of YAP expression in prostate cancer cells. Am J Transl Res. 2019;11:709.
37. Zhang Y, Wu X, Li Y, Zhang H, Li Z, Zhang Y, et al. Endothelial to mesenchymal transition contributes to arsenic-trioxide-induced cardiac fibrosis. Sci Rep. 2016;6:1–12.
38. Garelja ML, Bower RL, Brimble MA, Chand S, Harris PWR, Jamaluddin MA, et al. Pharmacological characterisation of mouse calcitonin and calcitonin receptor-like receptors reveals differences compared to human receptors. Br J Pharmacol. 2022;179:416–34.
39. Chang LL, Li YK, Zhao CX, Zeng CM, Ge FJ, Du JM, et al. Akr1c1 connects autophagy and oxidative stress by interacting with sqstm1 in a catalytic-independent manner. Acta Pharmacol Sin. 2022;43:703–11.
40. Orogo AM, Gustafsson ÅB. Therapeutic targeting of autophagy: potential and concerns in treating cardiovascular disease. Circ Res. 2015;116:489–503.
41. Liu Y, Hao C, Zhang W, Liu Y, Guo S, Li R, et al. Leucine-rich repeat kinase-2 deficiency protected against cardiac remodelling in mice via regulating autophagy formation and degradation. J Adv Res. 2022;37:107–17.
42. Shin JH, Park SJ, Jo DS, Park NY, Kim JB, Bae JE, et al. Down-regulated TMED10 in Alzheimer disease induces autophagy via ATG4B activation. Autophagy. 2019;15:1495–505.

Springer Nature or its licensor holds exclusive rights to this article under a publishing agreement with the author(s) or other rightsholder(s); author self-archiving of the accepted manuscript version of this article is solely governed by the terms of such publishing agreement and applicable law.